Polymer network-induced ordering in a nematogenic liquid: A Monte Carlo study

C. Chiccoli,[1] P. Pasini,[1] G. Skačej,[2] C. Zannoni,[3] and S. Žumer[2]

[1]*INFN, Sezione di Bologna, Via Irnerio 46, I-40126 Bologna, Italy*
[2]*Physics Department, University of Ljubljana, Jadranska 19, SI-1000 Ljubljana, Slovenia*
[3]*Dipartimento di Chimica Fisica ed Inorganica, Università di Bologna, Viale Risorgimento 4, I-40136 Bologna, Italy*

In this Monte Carlo study we investigate molecular ordering in a nematogenic liquid with dispersed polymer networks. The polymer network fibers are assumed to have rough surface morphology resulting in a partial randomness in anchoring conditions, while the fiber direction is assumed to be well defined. In particular, we focus on the loss of long-range aligning capability of the network when the degree of disorder in anchoring is increased. This process is monitored by calculating relevant order parameters and the corresponding ^{2}H nuclear magnetic resonance spectra, showing that the aligning ability of the network is lost only for completely disordering anchoring conditions. Moreover, above the nematic-isotropic transition temperature surface-induced paranematic order is detected. In addition, for perfectly smooth fiber surfaces with homeotropic anchoring conditions topological line defects can be observed.

PACS number(s): 61.30.Cz, 61.30.Gd

I. INTRODUCTION

Polymer networks dispersed in liquid crystals typically consist of thin fibers—a few nanometers thick—or of somewhat thicker fiber bundles. Having a rather high surface-to-volume ratio, polymer fibers can play a significant role in orienting the surrounding liquid crystal even if the polymer concentration in the sample is low [1–3]. Such composite systems are then similar to "ordinary" confined systems where liquid-crystalline ordering is affected by the interaction with the confining substrates (here substituted by fibers), external electric or magnetic fields, and by the disordering temperature effects. Therefore, composite materials such as liquid-crystal-dispersed polymer networks are interesting in themselves, as they are showing a variety of ordering and confinement-related phenomena. On the other hand, they are important also for the construction of electro-optical devices based on changing the orientation of liquid crystal molecules—initially imposed by the polymer network—by applying an aligning external electric field. Both the nature of this effect and the performance of electro-optical devices are intimately related to the anchoring and ordering conditions on the fiber surface, as well as to the topography of the network.

These network characteristics can be regulated during the polymerization from the monomer-liquid-crystal mixture through various parameters: monomer solubility, curing temperature, ultraviolet (UV) light curing intensity, and the degree of orientational ordering in the liquid-crystalline component [1]. In particular, poorly soluble monomers result in polymer fibers with a grainy and coarse surface morphology, while highly soluble monomers can form smooth fiber surfaces [4]. Further, high curing temperatures, as well as high UV light intensities, result in larger voids between polymer fibers [5]. If the liquid-crystalline component of the mixture is isotropic during the polymerization process, polymer fibers form directionless strands. On the other hand, performing the polymerization in the nematic phase, or applying an external aligning magnetic field, fibers can form bundles

with a well-defined average direction [1]. Similar types of networklike confinement can be achieved also in silica aerogel systems, where irregular chains of silica particles play the aligning role of polymer fibers [1]. While thin (nanometric) polymer fibers typically promote planar surface anchoring along the fiber direction, thicker fibers or fiber bundles (several 10 nm in diameter) can be treated with surfactants to yield homeotropic anchoring conditions.

Meanwhile there has been a growing number of experimental studies for these systems, e.g., measurements of optical transmission, capacitance, or ^{2}H nuclear magnetic resonance (NMR) spectroscopy [1–3,6]. They are usually accompanied by theoretical (Landau-de Gennes-type) analyses, but so far almost nothing has been done for such networklike confinement at the microscopic level. For all these reasons we decided to perform a thorough microscopic simulation study of the orientational coupling between polymer fibers and the surrounding liquid crystal. In this analysis we focused on polymer networks with a well-defined fiber net direction (as shown, for example, in Fig. 1 of Ref. [2]), and on effects of roughness on the fiber surface and the resulting randomness in surface anchoring. In this paper, we first briefly describe our model and the simulation method. Then we review changes in nematic ordering when the conditions on the fiber surface are varied from a perfectly aligning anchoring that imposes a well-defined orientation (planar along the fiber or homeotropic) to a completely disordering (random) anchoring. To complete our results, we calculate one of the possible experimental observables, the ^{2}H NMR spectra.

II. THE SIMULATION MODEL

The Monte Carlo (MC) simulations presented in this study are based on the Lebwohl-Lasher (LL) lattice model [7] in which uniaxial nematic molecules—or close-packed clusters containing up to 10^2 molecules [8]—are represented by unit vectors ("spins") $\mathbf{u}_i$. Despite the fact that the spins are fixed on the sites of a cubic lattice, the LL model is found to reproduce the orientational behavior of nematics suffi-

ciently well [9]. The interaction energy for a system of nematic particles is given by

$$U = -\sum_{\langle i<j \rangle} \epsilon_{ij} [\tfrac{3}{2} (\mathbf{u}_i \cdot \mathbf{u}_j)^2 - \tfrac{1}{2}], \qquad (1)$$

where ϵ_{ij} is a positive constant (ϵ if $\mathbf{u}_i$ and $\mathbf{u}_j$ are nearest neighbors, 0 otherwise).

As a first step towards modeling the complex topography of the polymer network, we considered a single straight cylindrical fiber oriented along the z axis. The shape of the fiber was defined by carving a "jagged" cylinder from the cubic lattice with lattice spacing a and taking all particles that are lying closer than R—the fiber radius—from the center of the xy plane. The particle orientations in the surface layer of the fiber ("ghost" spins) were chosen in agreement with the desired boundary conditions and were kept fixed during the simulation. The nematic-nematic and nematic-ghost interactions were chosen to be equal in strength, which corresponds to the strong anchoring limit [10]. We further assumed periodic boundary conditions at the simulation box boundaries. Such a setup, in fact, corresponds to a regular array of straight and parallel fibers.

In the case of "perfect" anchoring ghost spin orientations were chosen either along $\mathbf{z}$ (a unit vector along the z axis) for planar anchoring, or along the local radial unit vector for homeotropic anchoring. For cases with partially disordered anchoring the perfect planar or homeotropic ghost orientations were perturbed by performing an additional rotation for each of the ghost spins, characterized by a set of polar (θ) and azimuthal (ϕ) angles. While the ϕ angle was sampled from a uniform distribution within $[0, 2\pi]$, the sampling of θ (or, alternatively, $\cos \theta$) was biased so as to regulate the degree of randomness in ghost spin orientations. The biasing distribution was chosen to be $dw/d\cos\theta \propto \exp(A\cos^2\theta)$ (with w denoting the probability and $\cos \theta \in [-1,1]$), where for small A the resulting orientational distribution of ghosts becomes almost isotropic, while for large values of A it becomes strongly peaked at $\cos \theta = \pm 1$ (i.e., $\theta = 0$, π) and, therefore, approaches that of the perfect anchoring cases. In the case with completely disordering anchoring ghost orientations were sampled from a fully random orientational distribution. The degree of randomness can be given quantitatively by diagonalizing the ordering matrix $Q_{\alpha\beta} = \tfrac{1}{2}(3\langle u_i^\alpha u_i^\beta \rangle_g - \delta_{\alpha\beta})$ (the average $\langle \cdots \rangle_g$ taken over ghost spins), which gives the ghost director and the corresponding order parameter $\langle P_2 \rangle_g$. In all cases the $\langle P_2 \rangle_g$ order parameter is referred to as the z axis. Therefore, cases with $\langle P_2 \rangle_g = 1$ and $\langle P_2 \rangle_g = -0.5$ stand for perfect planar and homeotropic alignment, respectively, and $\langle P_2 \rangle_g \approx 0$ for a random orientational distribution. Intermediate values of $\langle P_2 \rangle_g$ then correspond to partial planar ($\langle P_2 \rangle_g > 0$) or partial homeotropic order ($\langle P_2 \rangle_g < 0$) in ghost orientations.

To study the radial dependence of order parameters, we found it convenient to divide our cubic simulation box into cylindrical layers surrounding the fiber (see Fig. 1). The observables accumulated during the production run were $\langle P_2^z \rangle$, quantifying the degree of ordering with respect to the z axis, $\langle P_2^c \rangle$, indicating how the order deviates from perfect radial
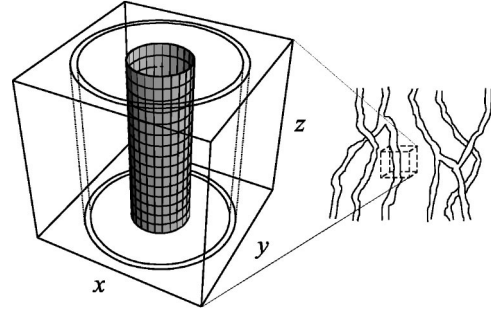

FIG. 1. Schematic depiction of the polymer network (right) and the simulation box with the cylindrical fiber and one of the cylindrical shells (left).

ordering in the xy plane, and the standard nematic order parameter S. Then, for example, $\langle P_2^z \rangle$ profiles were calculated as $\langle P_2^z \rangle (r) = \tfrac{1}{2}[3\langle (\mathbf{u}_i \cdot \mathbf{z})^2 \rangle_r - 1]$. The average $\langle \cdots \rangle_r$ has to be calculated over all nematic spins $\mathbf{u}_i$ belonging to the cylindrical layer with radius r, and over MC cycles. Analogously, $\langle P_2^c \rangle$ profiles were calculated with respect to the local unit vector $\mathbf{e}_r$, where $\mathbf{e}_r$ defines the local radial direction in the xy plane at the ith lattice site. Finally, the nematic order parameter profile $S(r)$ was obtained from the diagonalization of the ordering matrix $Q_{\alpha\beta}(r) = \tfrac{1}{2}(3\langle u_i^\alpha u_i^\beta \rangle_r - \delta_{\alpha\beta})$ averaged over sites in the nematic layer with radius r, and over MC cycles. The eigenvalue with the largest absolute value can then be identified as S and the difference between the remaining two eigenvalues corresponds to biaxiality.

In the absence of significant collective molecular reorientation during the MC evolution, it is instructive to calculate also the spatially resolved director and order parameter maps $\mathbf{n}(\mathbf{r}_i)$ and $S(\mathbf{r}_i)$, respectively, where $\mathbf{r}_i$ denotes the position of the ith lattice site. For this purpose the local ordering matrix $Q_{\alpha\beta}(\mathbf{r}_i) = \tfrac{1}{2}(3\langle u_i^\alpha u_i^\beta \rangle - \delta_{\alpha\beta})$ was averaged over MC cycles and then diagonalized, yielding the local value of the order parameter $S(\mathbf{r}_i)$, as discussed above, and the corresponding eigenvector, i.e., the local director $\mathbf{n}(\mathbf{r}_i)$. Similarly, the biaxiality map can also be deduced from the data.

In our simulation, the simulation box size was set to $30a \times 30a \times 30a$, which for the chosen fiber radius ($R = 5a$) amounts to 24 600 nematic and 840 ghost particles in total. Simulation runs were started from a completely random (disordered or isotropic) orientational configuration not to impose any preferred orientation in the system. Then the standard Metropolis scheme [11] was employed to perform updates in spin orientations [9,12]. Once the system was equilibrated (after at least 60 000 MC cycles), 66 000 (or more) successive spin configurations were used to calculate relevant observables. Results from MC simulations were expressed using selected order parameters and ^{2}H NMR spectra following the methodology presented in our earlier work on nematic droplets [13].

III. SIMULATION RESULTS

We report results obtained at two different reduced temperatures $T^* = kT/\epsilon$, $T^* = 1.0$ and $T^* = 1.2$, deep enough in the nematic and isotropic phases, respectively (the nematic-
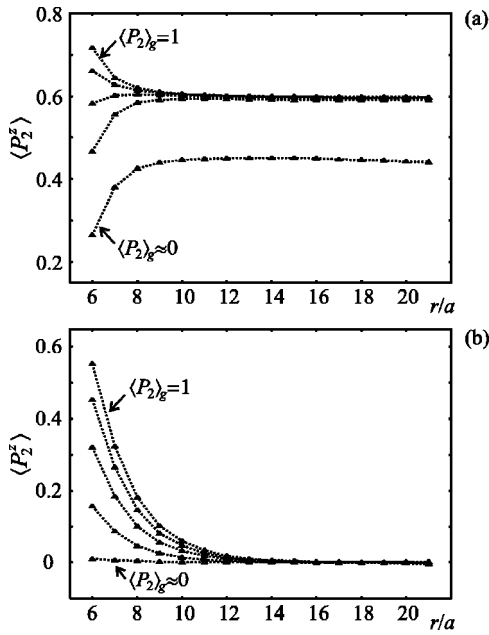
FIG. 2. Order parameter $\langle P_2^z \rangle$ vs r/a, the normalized distance from the simulation box center, as obtained from Monte Carlo simulations in a $30 \times 30 \times 30$ particle system, with a single cylindrical fiber of radius $R = 5a$ placed in the center of the simulation box. Planar anchoring along the z axis; (a) nematic ($T^* = 1.0$) and (b) isotropic phase ($T^* = 1.2$). In the plots each of the curves corresponds to a different degree of ordering in the ghost spin system: $\langle P_2 \rangle_g \approx 1.0$, 0.75, 0.50, 0.25, and 0 (top to bottom). The dotted lines serve as a guide to the eye (also in the following figures).

isotropic transition in the bulk takes place at $T^* = 1.1232$ [14]). Other calculations, not reported here for reasons of space, were performed at $T^* = 1.1$ with results qualitatively similar to those obtained for $T^* = 1.0$. The correlation length for orientational ordering at these temperatures was found not to exceed ≈ 5 lattice spacings a, which with our choice for the simulation box size is expected to be enough to avoid spurious correlations originating from periodic boundary conditions. In this study the fiber radius was fixed to $R = 5a$. Another set of runs for a thinner fiber with $R = 3a$ has also been performed, but has shown no major difference in comparison with the $R = 5a$ case and is, therefore, not reported here.

A. Planar alignment ($\|z$), nematic phase

The first case we have treated is a nematic sample at $T^* = 1.0$, with planar anchoring along the z direction and with possible deviations from this perfect alignment, as described above. This situation corresponds to a series of polymer fibers whose surface morphology varies from smooth to rough and disordered. In Fig. 2(a) we present how the $\langle P_2^z \rangle$ order parameter changes across the simulation box from the fiber surface to the outer sample boundaries. Different curves shown in the plot correspond to different degrees of order in the ghost spin system, $\langle P_2 \rangle_g$. For perfect planar anchoring $\|z$ with $\langle P_2 \rangle_g = 1$ the nematic director $\mathbf{n}$ is parallel to z. In this case $\langle P_2^z \rangle$ becomes a direct measure for S because $\mathbf{n}$ and
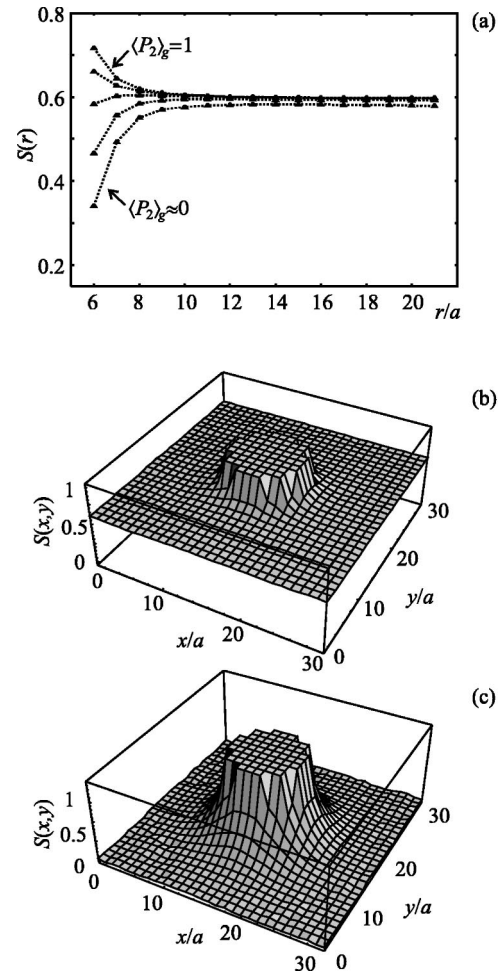

FIG. 3. Planar anchoring $\|z$. (a) Order parameter radial profiles $S(r)$ for different values of $\langle P_2 \rangle_g$ in the nematic phase ($T^* = 1.0$); curves are labeled like in Fig. 2. (b) Perfect planar anchoring ($\langle P_2 \rangle_g = 1$); xy cross section of the local $S(\mathbf{r}_i)$ order parameter map in the nematic phase ($T^* = 1.0$). (c) Same as (b), but in the isotropic phase ($T^* = 1.2$).

z coincide. Far enough from the fiber the value of $\langle P_2^z \rangle$ approaches ≈ 0.6, matching with the value of S in a bulk sample at $T^* = 1.0$ [14], while close to the fiber there is an increase in $\langle P_2^z \rangle$ reflecting the fiber-induced enhancement of nematic order. The same effect is further confirmed by the behavior of the $S(r)$ profile depicted in Fig. 3(a), as well as by the $S(x,y)$ local order parameter map shown in Fig. 3(b). For all three profiles the characteristic length of the nematic order variation ξ roughly amounts to $\approx 3a$.

Studying cases with reduced (imperfect) planar anchoring $\|z$ [Figs. 2(a) and 3(a)], one can see that at least down to $\langle P_2 \rangle_g \approx 0.25$ the bulk value of both order parameters remains essentially unchanged if compared to the perfect $\langle P_2 \rangle_g = 1$ case. Note that now for, e.g., $\langle P_2 \rangle_g \approx 0.75$ the increase of order close to the fiber is smaller than for $\langle P_2 \rangle_g = 1$, and that already for $\langle P_2 \rangle_g \approx 0.50$ (as well as for $\langle P_2 \rangle_g \approx 0.25$) the surface degree of order is somewhat lower than its bulk value. From these observations one can conclude that the first effect of the partial disorder in surface anchoring is merely a slight decrease in the degree of nematic order in the vicinity of the
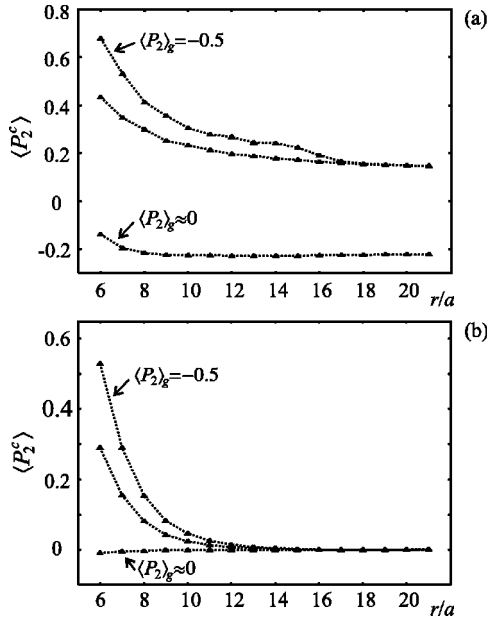
FIG. 4. Order parameter profiles $\langle P_2^c \rangle$ for homeotropic anchoring with $\langle P_2 \rangle_g \approx -0.50$, -0.25, and 0 (top to bottom); (a) nematic phase ($T^* = 1.0$) and (b) isotropic phase ($T^* = 1.2$).
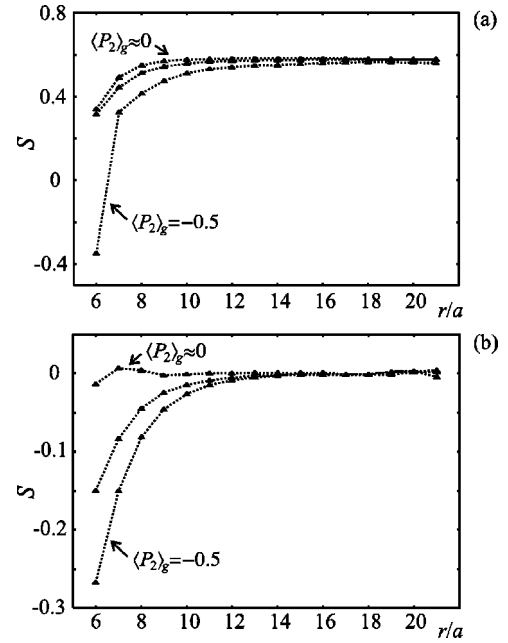

FIG. 5. Order parameter profiles $S(r)$ for homeotropic anchoring. Curve labels are same as in Fig. 4. (a) Nematic phase ($T^* = 1.0$) and (b) isotropic phase ($T^* = 1.2$).

fiber, but that at this point the long-range orienting ability of the polymer network is not lost. This ability, however, weakens upon further decreasing $\langle P_2 \rangle_g$, but is present at least down to $\langle P_2 \rangle_g \approx 0.09$ (the corresponding profiles not plotted here). Then only in a sample with a completely disordering fiber—for $\langle P_2 \rangle_g \approx 0$—the net orientation of the nematic for our intermolecular potential is completely detached from the fiber direction. This follows from the behavior of the $\langle P_2^z \rangle$ order parameter (calculated with respect to the fixed fiber direction) which now, in principle, can take any arbitrary value, and from the fact that the liquid crystal is still nematic, as suggested by a nonzero value of the S order parameter throughout the sample. Note that the bulk value of S remains almost unaltered in comparison to, e.g., the $\langle P_2 \rangle_g = 1$ case. The fact that it is actually slightly lower than the value obtained for $\langle P_2 \rangle_g = 1$ (≈ 0.6) can be attributed to slow collective molecular motion during the production run.

B. Homeotropic alignment, nematic phase

If we now proceed to cases with $\langle P_2 \rangle_g < 0$, i.e., to perturbed homeotropic ordering, already for $\langle P_2 \rangle_g \approx -0.08$ the polymer fiber is able to align the liquid crystal. Molecules are now aligned perpendicular to z, the fiber direction, i.e., mainly within the xy plane. This can be deduced from $\langle P_2^z \rangle$ profiles; the $\langle P_2^z \rangle$ values being now negative for all r (not plotted here). Similarly as for planar anchoring there is a decrease in the degree of nematic ordering close to the fiber, e.g., for $\langle P_2 \rangle_g \approx -0.25$ (partial disorder) and an enhancement for $\langle P_2 \rangle_g = -0.50$ (perfect homeotropic order). Studying cases with homeotropic surface alignment, it is more convenient to plot the $\langle P_2^c \rangle$ order parameter profiles. Note now that for $\langle P_2 \rangle_g = -0.50$ the $\langle P_2^c \rangle$ profile—shown in Fig. 4(a)—is always positive and that the $\langle P_2^c \rangle$ values are rather

high close to the fiber. This is a signature of strong radial ordering, along with the negative values of S in the first layer next to the fiber surface, see Fig. 5(a). Going away from the fiber, $\langle P_2^c \rangle$ exhibits a plateaulike behavior, before relaxing to the bulk value close to $\approx S/4$, which is characteristic for homogeneous (undeformed) nematic ordering. Such alignment far from the fiber is compatible with strong radial ordering in the fiber vicinity only if topological defects are to form. In fact, as shown in the director map $\mathbf{n}(\mathbf{r}_i)$, Fig. 6(a), a pair of $-\frac{1}{2}$ strength defect lines forms along the fiber and close to the simulation box diagonal. The plateau in $\langle P_2^c \rangle$ profiles then corresponds to the distortion of the director field imposed by the defect lines. In the vicinity of the lines there is a strong change in the degree of nematic order S (it even becomes negative), with the director pointing out of xy plane [Figs. 6(a) and 6(d)]. Further, in this region molecular ordering is accompanied also by non-negligible biaxiality. The inner structure of the defect lines was studied in more detail elsewhere [15].

There are two parameters characterizing the position of each defect line: its distance from the fiber surface and the corresponding polar angle in the xy plane. Increasing the system temperature from $T^* = 1.0$ to $T^* = 1.1$, the pair of defect lines moves away from the fiber, which increases the thickness of the deformed region where radial ordering is well pronounced, as imposed by strong surface anchoring; compare Figs. 6(a) and 6(b). This can be deduced also from the $S(r)$ profile, Fig. 7, where radial ordering reflects in $S(r) < 0$ close enough to the fiber. The increase of T^* results in an overall decrease of S and, consequently, in a decrease of the corresponding elastic constants (proportional to S^2). Moreover, when approaching the fiber surface, at higher T^* the increase in S is larger and occurs over a somewhat larger
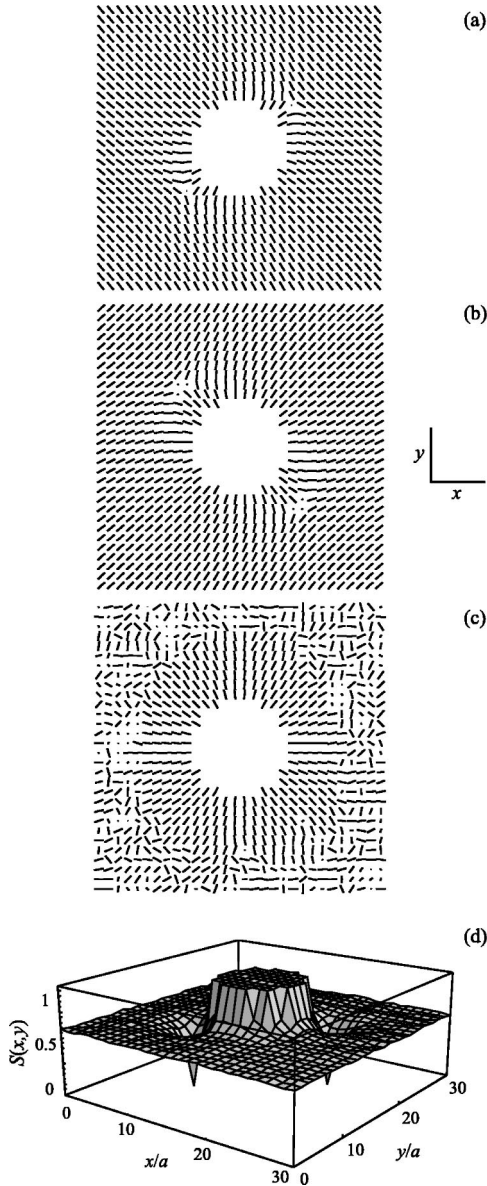
FIG. 6. Director field for perfect homeotropic anchoring, xy cross section. (a) $T^*=1.0$, (b) $T^*=1.1$ (both nematic), and (c) $T^*=1.2$ (isotropic phase). (d) xy cross section of the $S(\mathbf{r}_i)$ order parameter map for $T^*=1.0$. In the nematic phase a pair of $-\frac{1}{2}$ strength defects has formed close to the diagonal.

characteristic length ξ, which makes the defect formation and the accompanying elastic deformation in the immediate fiber vicinity rather unfavorable. Therefore, the defects are pushed away from the fiber surface when T^* is increased. On the other hand, according to our tests, at fixed T^* the defects move away from the fiber also as the fiber radius R is increased. In addition, for a given R the defect-to-fiber distance seems to be rather insensitive to changing the simulation box size. Indeed, for large R (i.e., for a low curvature of the fiber surface) the elastic deformation imposed by the defect is more compatible with the radial aligning tendency of the fiber if the defect is located far enough from the fiber surface. Finally, for our system size the main mechanism for the formation of the defects close to the simulation box diagonal
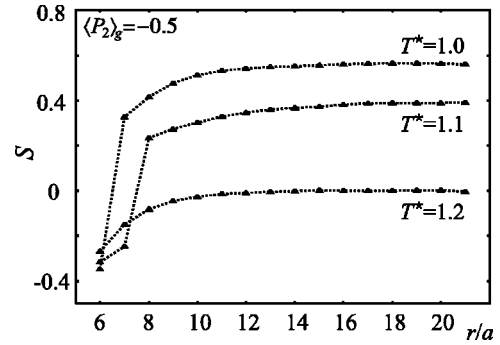

FIG. 7. Order parameter profiles $S(r)$ for perfect homeotropic anchoring and different temperatures. With increasing T^* the defects move away from the fiber [compare with Figs. 6(a) and 6(b)].

seems to be the repulsion between defects corresponding to adjacent fibers. This mechanism is possibly enhanced by collective fluctuations, as mentioned in Ref. [15]. Also the defect-to-defect repulsion is mediated by curvature elasticity and weakens upon increasing temperature. The actual defect position is then determined by the subtle interplay between all the effects listed above. Note that for $T^*\lesssim 1$ the defect position becomes almost temperature independent. Note also that the defect size increases with temperature, which qualitatively agrees with an increase of the characteristic length ξ on approaching the nematic-isotropic transition.

C. Planar alignment ($\|z$), isotropic phase

If temperature in the LL model is further increased to $T^*=1.2$, in a bulk sample the isotropic phase is stable. However, in restricted space, aligning substrates can induce nematic ordering even at temperatures well above the nematic-isotropic transition. The same phenomenon is expected also in a nematic with a dispersed polymer network. For the case of planar anchoring $\|z$ Figs. 2(b) and 3(c) show the $\langle P_2^z \rangle$ and the local $S(x,y)$ profiles, and in fact confirm the existence of surface-induced planar ordering. Note that the layer-averaged nematic order parameter profile $S(r)$ would have looked exactly like the $\langle P_2^z \rangle$ profile and is, therefore, not shown here. The net molecular orientation is still along $\mathbf{z}$, as imposed by the fiber, and the corresponding degree of order (given either by $\langle P_2^z \rangle$ or S) decays to zero over a characteristic length of the order of $\xi \approx 5a$.

D. Homeotropic alignment, isotropic phase

Analogous conclusions as for planar anchoring can be drawn in the isotropic phase also for the homeotropic case, now inspecting the decays in $\langle P_2^c \rangle$ and S order parameters shown in Figs. 4(b) and 5(b). Note that the two defect lines observed in the nematic phase for $T^*=1.0$ and $T^*=1.1$ have now vanished and that the residual surface-induced ordering is simply radial [Fig. 6(c)]. This is because the fiber-to-fiber distance in our simulation is larger than 2ξ and the degree of ordering at the simulation box boundaries is already negligibly small. Consequently, no relevance should be attributed to the "randomly" distributed directors plotted in the outer cylindrical layers of the sample, Fig. 6(c).
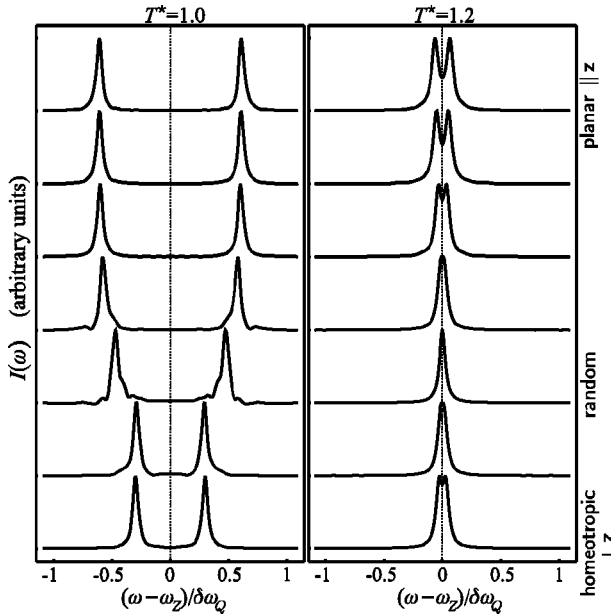
FIG. 8. ^{2}H NMR spectra; $T^*=1.0$ (left) and $T^*=1.2$ (right). Top to bottom: spectra for $\langle P_2 \rangle_g = 1.0$, 0.75, 0.50, 0.25, 0, -0.25, and -0.50. ω_Z denotes the Zeeman frequency and $\omega_Q = \omega - \omega_Z$.

IV. SIMULATIONS OF ^{2}H NMR SPECTRA

The observations listed in the preceding section can be confirmed also by calculating ^{2}H NMR spectra using the numerical output from MC simulations. Experimentally, ^{2}H NMR is one of the most convenient tools for investigating confined liquid-crystalline samples [1]. As discussed elsewhere [1,13], in deuterated nematics quadrupolar interactions perturb the Zeeman energy levels and give rise to a molecular orientation-dependent frequency splitting in the NMR spectrum. In uniaxial nematics it is given by $\omega_Q(\mathbf{r}) = \pm \frac{1}{2} \delta \omega_Q S(\mathbf{r}) [3 \cos^2 \theta(\mathbf{r}) - 1]$, where $\delta \omega_Q$ is the quadrupolar coupling constant (typically $\approx 2\pi \times 40$ kHz), $S(\mathbf{r})$ the local uniaxial nematic order parameter, and $\theta(\mathbf{r})$ the angle between the local nematic director and the NMR spectrometer magnetic field. Figure 8 shows the NMR spectra calculated for the $30 \times 30 \times 30$ particle sample and a single fiber in the nematic (left) and in the isotropic phase (right), with the spectrometer field applied along the fiber direction $\mathbf{z}$. The calculation was based on generating the free induction decay (FID) signal from the MC data and calculating its Fourier transform representing the spectrum, as described in detail in Ref. [13]. Generating the FID signal, we also included effects of translational diffusion, which always becomes important in strongly confined systems. Following Ref. [13], the diffusive molecular motion was simulated by a random walk on the cubic lattice, performing 1024 diffusion steps per NMR cycle. The effective diffusion constant for such a random-walk process can be measured to be $D = 256 a^2 \delta \omega_Q / 3\pi$, yielding a root-mean-square molecular displacement of $\sqrt{6 D t_0} = 32a$ in each NMR cycle. Here a stands for the spin-to-spin spacing on the cubic lattice, while $t_0 = 2\pi / \delta \omega_Q$ denotes the NMR cycle duration. Since this displacement is comparable to the size of our sample, the calculated NMR spectra are expected to be highly diffusion

averaged. Finally, note that the NMR spectrometer magnetic field is assumed to be weak enough not to align nematic molecules, which, again, is the case only for strongly confined systems.

The calculated spectra are shown in Fig. 8, left. In the nematic phase with $T^*=1.0$, for perfect planar anchoring ($\langle P_2 \rangle_g = 1$) in the spectrum we have two peaks positioned at $\omega_Q / \delta \omega_Q \approx 0.6$. In the geometry we chose, $\omega_Q / \delta \omega_Q$ is supposed to be roughly equal to the value of S, the nematic order parameter, since the director and the direction of the NMR spectrometer magnetic field coincide. Indeed, for $T^*=1.0$ we have $S \approx 0.6$, as already seen above from various order parameter profiles. Translational diffusion in this case affects the spectra only negligibly: the nematic director is homogeneous throughout the sample and the degree of order is enhanced only slightly in the vicinity of the fiber. Therefore, the effect of diffusion should be merely a slight increase in quadrupolar splitting, but the resolution of our spectra is not high enough to clearly see this surface ordering-induced shift.

Proceeding now to fibers with partially disordered anchoring, in the spectra there is no major change at least down to $\langle P_2 \rangle_g \approx 0.25$, reflecting the ability of the polymer network to align the surrounding liquid crystal along $\mathbf{z}$. In the case when anchoring is completely disordered and $\langle P_2 \rangle_g \approx 0$ holds, the spectrum typically still consists of two peaks, however, the corresponding splitting can be arbitrary because there is no preferred direction in the system—note that only one example of the possible spectra is plotted. Note also that sometimes during the acquisition of the FID signal slow collective molecular motion can occur, which results in an increase of the spectral linewidth. On the other hand, in homeotropic cases with $\langle P_2 \rangle_g \lesssim 0$, molecular ordering is confined to the xy plane. The quadrupolar splitting now decreases by 50% with respect to perfect planar anchoring because the director is perpendicular to the spectrometer field direction (see the two spectra in the bottom of Fig. 8, left).

In the bulk isotropic phase, however, quadrupolar interactions giving rise to the ω_Q splitting are averaged out by the rapid molecular motion. Therefore, ignoring translational diffusion, in a confined system for $S \approx 0$ one should expect a single-peaked spectrum at $\omega_Q \approx 0$, as already suggested above, and somewhat broadened by the surface-induced order. The spectra shown in Fig. 8, right, were calculated with fast translational diffusion, and it is evident that some of them are actually double peaked. This is a clear signature of surface-induced paranematic order. In fact, the peak-to-peak distance decreases with decreasing degree of surface order; compare with Figs. 2(b) and 5(b). For $\langle P_2 \rangle_g \approx 0$ exhibiting no surface order, the spectrum is again single peaked. Finally, note that the splitting observed for perfect planar anchoring ($\langle P_2 \rangle_g = 1$) roughly amounts to twice the splitting seen in the perfectly homeotropic case ($\langle P_2 \rangle_g = -0.5$). This is because the nematic director close to the fiber is parallel to the NMR spectrometer magnetic field in the first case and perpendicular to the field in the second.

V. CONCLUSION

We have performed a Monte Carlo analysis of the aligning effect imposed by a polymer network dispersed in a

liquid-crystalline material. To model the liquid crystal we have adopted a simple lattice model based on microscopic interactions, which turned out to be suitable for the description of ordering induced by polymer fibers. Different types of anchoring conditions on the fiber surface have been considered: planar along the fiber direction, homeotropic, and partially or completely random. In cases with perfect planar or homeotropic anchoring in the very vicinity of the fiber nematic order is enhanced. However, once the anchoring conditions are partially distorted, the surface degree of nematic order may drop below its bulk value, but the long-range orienting capability of the fiber network is still retained. This ability seems to be lost only for completely random anchoring imposing no well-defined direction in the system, as confirmed also by the ^{2}H NMR spectra calculated from the simulation output. Further, above the nematic-isotropic transition surface-induced paranematic ordering has been detected, reflecting clearly in the translational diffusion-averaged ^{2}H NMR spectra. In addition, in the nematic phase two $-\frac{1}{2}$ strength disclination lines parallel to the fiber were observed for perfect homeotropic anchoring, and were seen to move away from the fiber upon increasing temperature. We believe that the simplified topography of the fiber network does not affect the qualitative character of our conclusions, at least for low-density polymer networks. More realistic network models should include curved fibers positioned randomly inside the simulation box and allow for cross linking between them at higher concentrations.

[1] G. P. Crawford and S. Žumer, *Liquid Crystals in Complex Geometries Formed by Polymer and Porous Networks* (Taylor & Francis, London 1996).

[2] Y. K. Fung, A. Borštnik, S. Žumer, D.-K. Yang, and J. W. Doane, Phys. Rev. E **55**, 1637 (1997).

[3] R.-Q. Ma and D.-K. Yang, Phys. Rev. E **61**, 1567 (2000).

[4] I. Dierking, L. L. Kosbar, A. Afzali-Ardakani, A. C. Lowe, and G. A. Held, Appl. Phys. Lett. **71**, 2454 (1997).

[5] I. Dierking, L. L. Kosbar, A. C. Lowe, and G. A. Held, Liq. Cryst. **24**, 397 (1998); **24**, 387 (1998).

[6] M. J. Escuti, C. C. Bowley, G. P. Crawford, and S. Žumer, Appl. Phys. Lett. **75**, 3264 (1999).

[7] P. A. Lebwohl and G. Lasher, Phys. Rev. A **6**, 426 (1972).

[8] C. Chiccoli, P. Pasini, F. Semeria, E. Berggren, and C. Zannoni, Mol. Cryst. Liq. Cryst. Sci. Technol., Sect. A **266**, 241 (1995).

[9] *Advances in the Computer Simulations of Liquid Crystals*, edited by P. Pasini and C. Zannoni (Kluwer, Dordrecht, 2000).

[10] N. Priezjev and R. A. Pelcovits, Phys. Rev. E **62**, 6734 (2000).

[11] N. Metropolis, A. W. Rosenbluth, M. N. Rosenbluth, A. H. Teller, and E. Teller, J. Chem. Phys. **21**, 1087 (1953).

[12] J. A. Barker and R. O. Watts, Chem. Phys. Lett. **3**, 144 (1969).

[13] C. Chiccoli, P. Pasini, G. Skačej, C. Zannoni, and S. Žumer, Phys. Rev. E **60**, 4219 (1999); **62**, 3766 (2000).

[14] U. Fabbri and C. Zannoni, Mol. Phys. **58**, 763 (1986).

[15] D. Andrienko, M. P. Allen, G. Skačej, and S. Žumer, Phys. Rev. E **65**, 041702 (2002).